actuators

MDPI

*Article*

# Design of Tendon-Driven Mechanism Using Geometrical Condition

**Takashi Takuma**

Department of Electric and Electrical System Engineering, Osaka Institute of Technology, Osaka 5358585, Japan; takashi.takuma@oit.ac.jp

Received: 24 April 2020; Accepted: 18 June 2020; Published: 30 June 2020

**Abstract:** A tendon-driven robot offers many advantages, such as easy designs for mass distribution that facilitate dexterous motion. A procedure to design such a robot using a single actuator to achieve the desired force direction and magnitude on an endpoint is presented herein. The force on the endpoint is generated by the single actuator and a wire that passes through pulleys attached on links. To set the pulley position for the desired force direction and magnitude, a geometrical condition is proposed. To evaluate the proposed method, a physical monopod robot was developed. We compared the calculated and physical forces on the endpoint of the physical robot for the desired directions. Finally, we confirmed that the proposed method provided the desired force on the endpoint without iterative trials.

**Keywords:** tendon-driven robot; pulley position; operation of direction and amount of force at endpoint

## 1. Introduction

Wire- or tendon-driven robots whose joints are driven through a wire have been discussed extensively in the field of robotics. Many manipulators and hands are driven by wires [1–5]. Higashimori et al. explained a wire-driven mechanism wherein multiple joints are driven by a single actuator [2]. An advantage of the wire- or tendon-driven mechanism is that an actuator is set apart from the joint. In a robot finger, the volume of the finger is limited, and it is difficult to set an actuator to drive the finger joint in the finger link.

Some researchers have developed legged robots driven by wires [6–8]. In the tendon-driven mechanism, multiple joints are driven simultaneously by pulling a wire that passes through points, e.g., pulleys attached on links. Therefore, the number of actuators, as well as the mass and inertia, of the leg link can be reduced. Seok and Kim et al. indicated that the mass and inertia should be small to swing the leg for faster locomotion [9]. For a jumping robot in which all joints are individually driven by actuators, a large landing impact occurs due to the heavy mass of the actuators that causes the joint and actuator to break. Meanwhile, a tendon-driven mechanism with a small number of actuators can avoid the generation of such a heavy landing impact.

The tendon-driven mechanism has been extensively investigated; it typically involves setting the pulley position symmetrical to the joint or the center of the link to facilitate a simple calculation of the robot posture and force [10–12]. It has been indicated that the pulley position affects the robot motion because the force of the wire is added to the pulley and the joint torque in a rotational joint is changed by the pulley position. Higashimori et al. derived an equation for the tendon-driven mechanism that explains the relationship between the pulley position and each joint torque [2]. In some studies, the pulley position or the wire routing have been determined by iterative trials [13–16] because the mechanism of the motion is extremely complex; consequently, it is difficult to explain the relationship between task performance and pulley position using a formula. Chen et al. optimized

the position or radius of a pulley to obtain force equilibrium using a numerical model [13]. Though this approach provides the optimized pulley position, it requires iterative trials that cause the joints and pulley of a physical robot to break. Researchers have investigated the optimal pulley position that provides the desired vertical force for the successful jumping of a one-legged robot by analyzing all possible pulley positions [14]. However, similar to the work of [13], iterative trials are required.

In this study, a single-legged robot in which all joints were driven by a single actuator and a wire passed through the robot was used. A model of the tendon-driven mechanism was adopted by revising the Higashimori tendon-driven mechanism [2], and a geometrical condition to determine the pulley position was derived. This method provides the desired force direction and magnitude on the toe without iterative trials. It determines the pulley position by referring to a figure that indicates the robot's posture. Therefore, the position was simply and intuitively determined during the design phase of the robot. To confirm the effect of the proposed method, this approach was applied to vertical jumping that only required a vertical force to the ground. Furthermore, we demonstrated that the direction of the force on the endpoint, or the toe in this study, could be arbitrarily determined by setting the pulley position. For verification, a physical legged robot was developed, and the robot was observed to verify whether it successful achieved vertical jumping. Additionally, we observed whether the desired force was generated at the endpoint of the foot.

## 2. Robot Model

### *2.1. Framework and Tendon-Driven Mechanism*

Figure 1a shows the frame of the robot and driving mechanism, which is comprised of a single actuator and wire set. Figure 1b shows the pulley position based on the coordinate system, $\Sigma_k$: The origin was set on the tips of the foot; the $X_k$-axis was set along the foot link; and the $Y_k$-axis was perpendicular to the $X_k$-axis. The model had four links, i.e., trunk, thigh, shank, and foot, as well as three joints, i.e., hip, knee, and ankle. The lengths of the links are denoted by $l_1$–$l_4$, and the torques of the hip, knee, and ankle are denoted by $\tau_1, \tau_2$, and $\tau_3$, respectively. The angle is denoted by $\theta_1, \theta_2$, and $\theta_3$. To derive the relationship between the pulley position and reaction force, the coordinate system, $\Sigma_0$, was set as follows: The origin was set on the tips of the trunk, the $Y_0$-axis was set along the trunk link, and the $X_0$-axis was set perpendicular to the $Y_0$-axis, as shown in Figure 1b. The positions of the pulley and endpoint of the wire are labeled $P_i$ (i = 0, 1, 2, 3), and the joints are labeled $J_i$ (i = 1, 2, 3). The point where the wire was attached to the actuator is $P_0$, and the other endpoint of the wire is $P_3$. $P_1$ and $P_2$ were attached to the thigh and shank link, respectively. $P_0$ is the tip of the rod of the linear actuator, and the actual point moved when the linear actuator pulled the wire. Because this paper discusses the force at the moment when the actuator drives and pulls the wire and because the distance of the movement is short compared with the size of the links, we assumed that point $P_0$ did not move when the actuator was driven in the coordinate system, $\Sigma_0$. $J_1$, $J_2$, and $J_3$ correspond to the hip, knee, and ankle joints, respectively. $e_i$ (i = 1, 2, 3) is the unit vector of the tensional force on pulley $P_i$, and T is the pulling force magnitude of the actuator.

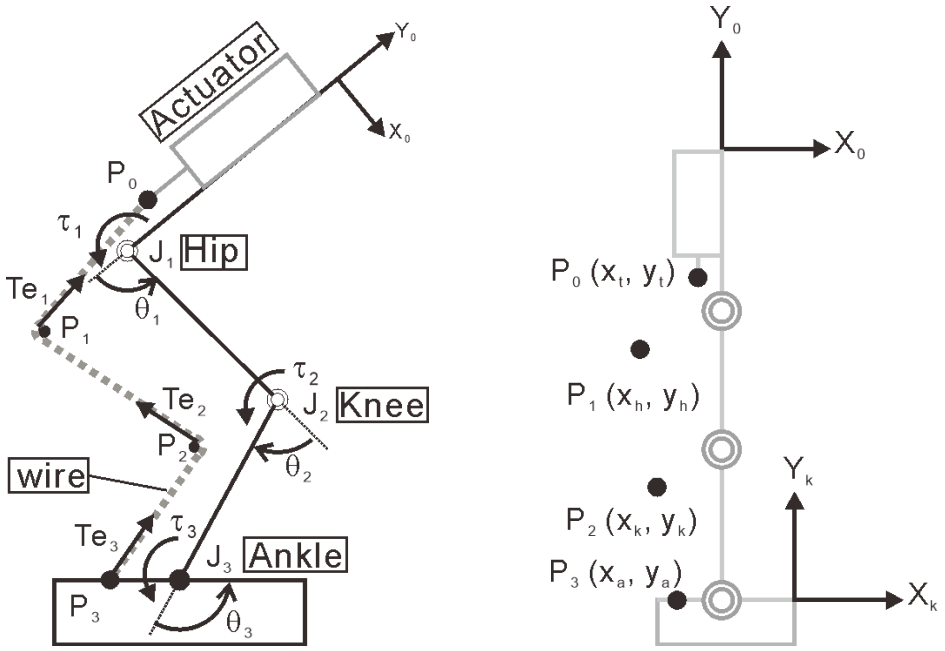


(**a**) (**b**)

**Figure 1.** Joint configuration and position of pulley. (**a**) Wire, pulley, and joint configuration; (**b**) Pulley position with respect to the coordinate system ($\Sigma_k$).

*2.2. Mathematical Model*

Figure 2a shows the relationship between the joint torques and force on the toe. The horizontal and vertical forces generated by the joint torque are expressed as $F_x$ and $F_y$, respectively. Following the principle of virtual work, the relationship between the joint torque, $(\tau_1, \tau_2, \tau_3)^T$, and $(F_x, F_y)^T$, is expressed as:

$$\boldsymbol{\tau} = \begin{pmatrix} \tau_1 \\ \tau_2 \\ \tau_3 \end{pmatrix} = \mathrm{J}^{\mathrm{T}}\mathrm{R}\begin{pmatrix} F_x \\ F_y \end{pmatrix}, \mathrm{J} = \begin{pmatrix} \frac{\partial x}{\partial \theta_1} & \frac{\partial x}{\partial \theta_2} & \frac{\partial x}{\partial \theta_3} \\ \frac{\partial y}{\partial \theta_1} & \frac{\partial y}{\partial \theta_2} & \frac{\partial y}{\partial \theta_3} \end{pmatrix}, \quad (1)$$

where $(x, y)$, which is the position of the toe in the coordinate system, $\Sigma_0$, is expressed as follows:

$$x = l_2 \sin\theta_1 + l_3 \sin(\theta_1 + \theta_2) + l_4 \sin(\theta_1 + \theta_2 + \theta_3),$$
$$y = -l_1 - l_2 \cos\theta_1 - l_3 \cos(\theta_1 + \theta_2) - l_4 \cos(\theta_1 + \theta_2 + \theta_3).$$

where R is the rotation matrix for addressing the force, $(F_x, F_y)^T$ in $\Sigma_0$; it is expressed as follows:

$$\mathrm{R} = \begin{pmatrix} \sin\Theta & \cos\Theta \\ -\cos\Theta & \sin\Theta \end{pmatrix}, \Theta = \theta_1 + \theta_2 + \theta_3$$

The joints were driven by the force applied to the pulley. The joint torque was determined by the amount of pulling force $T$, the length of moment arm between the joint and pulley, and the angle between the moment arm and the direction of pulling force, as shown in Figure 2b. Higashimori et al. derived the torques for such a tendon-driven mechanism with a single wire and an actuator [2]. In their study, the radius of the pulley was assumed to be nonzero, i.e., the pulley was assumed to have a certain volume. For a simple expression, extremely thin pin-shaped pulleys were used in this study, and it was assumed that the radius of the pulley was infinitely small or approximately zero. Following this assumption, the relationship between the pulley position and torques can be expressed by modifying Higashimori's equation as follows:

$$\begin{pmatrix} \tau_1 \\ \tau_2 \\ \tau_3 \end{pmatrix} = -T\begin{pmatrix} (\mathbf{p_1} - \mathbf{j_1}) \otimes \mathbf{e_1} - (\mathbf{p_2} - \mathbf{j_2}) \otimes \mathbf{e_2} \\ (\mathbf{p_2} - \mathbf{j_2}) \otimes \mathbf{e_2} - (\mathbf{p_3} - \mathbf{j_3}) \otimes \mathbf{e_3} \\ (\mathbf{p_3} - \mathbf{j_3}) \otimes \mathbf{e_3} \end{pmatrix}, \quad (2)$$

where $\mathbf{p_i}$ (i = 1, 2, 3) is the position vector of $P_i$, $\mathbf{j_i}$ is that of joint $J_i$, and $e_i$ is the unit vector from $P_i$ to $P_{i-1}$ (see Figure 1a). The operator, $\otimes$, was used as follows:

$$(x_1, y_1)^T \otimes (x_2, y_2) = x_1 y_2 - y_1 x_2.$$

By combining Equations (1) and (2), the relationship between force ($F_x$, $F_y$) and pulley position $P_i$ can be explained.

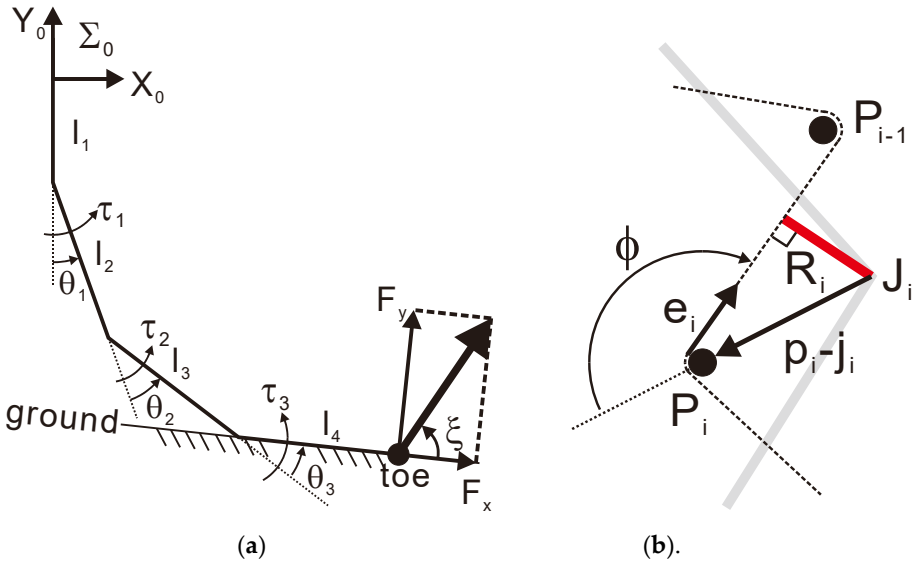


(**a**) (**b**).

**Figure 2.** Mathematical model. (**a**) Posture and force; (**b**) Distance $R_i$.

*2.3. Geometrical Condition for Desired Force Direction and Magnitude on the Endpoint*

Considering that vector $e_i$ in Equation (2) is the unit vector, the term $(\mathbf{p_i} - \mathbf{j_i}) \otimes \mathbf{e_i}$ (i = 1, 2, 3) in Equation (2) is deformed to the following:

$$(\mathbf{p_i} - \mathbf{j_i}) \otimes \mathbf{e_i} = |\mathbf{p_i} - \mathbf{j_i}| \sin\phi \triangleq R_i, \qquad (3)$$

where $\phi$ is the angle between $\mathbf{p_i} - \mathbf{j_i}$ and $\mathbf{e_i}$ (see Figure 2b). Therefore, the term $R_i$ is expressed as the length between the lines of $P_{i-1}$ and $P_i$ and the joint $J_i$. By expressing forces $F_x$ and $F_y$ as $F_x = F\cos\xi$ and $F_y = F\sin\xi$, where $F$ is the magnitude of the force, i.e., $F = \sqrt{F_x^2 + F_y^2}$, and $\xi$ is direction of the force, as shown in Figure 2. The combination of Equations (1), (2), and (3) is expressed as follows:

$$\begin{pmatrix} R_1 - R_2 \\ R_2 - R_3 \\ R_3 \end{pmatrix} = K\mathrm{J}^{\mathrm{T}}\mathrm{R}\begin{pmatrix} \cos\xi \\ \sin\xi \end{pmatrix}, \qquad (4)$$

where $K = -F/T$ is the ratio of the pulling wire force, $T$, and the force magnitude, $F$. By determining $\xi$, which depends on the behavior type such as vertical jumping, $R_i$ ($i$ = 1, 2, 3) was calculated. Considering that $R_i$ is the distance from the joint to line $P_i$–$P_{i-1}$, line $P_i$–$P_{i-1}$ was determined by calculating $R_i$ such that the line was tangent to the circle whose radius was $R_i$ and whose origin was joint $J_i$, as shown in Figure 2b. From the third row, length $R_3$ was obtained when K and joint angles were determined. From the second row, $R_2$ was automatically obtained. From the first row, $R_3$ was obtained. Because the positions of terminal points, $P_0$ and $P_3$, were fixed, the positions of $P_1$ and $P_2$ were constrained by the conditions of $R_1$, $R_2$, and $R_3$. Using such geometrical conditions, the pulley position that generated the desired force on the toe can be derived as follows:

1. Set angles $\theta_i$ (i = 1, 2, 3) that satisfy the condition of the behavior.
2. Calculate the constant value, $K = -F/T$, by determining $F$ and $T$.
3. Set circle $C_i$ (i = 1, 2, 3), whose radius is $R_i$ and center is joint $J_i$ (see Figure 3).
4. Set line $t_1$ that is tangent to circle $C_1$ and passes through $P_0$. $t_1$ is the set of candidates of pulley positions $P_1$.
5. Set line $t_3$ that is tangent to circle $C_3$ and passes through $P_3$. $t_3$ is the set of candidates of pulley positions $P_2$.

6. Pulley position $P_1$ is determined on line $t_1$, or position $P_2$ is determined on line $t_3$.

6-1. When $P_1$ is determined, line $t_2$ that is tangent to circle $C_2$ and passes through $P_1$ is set, and $P_2$ is determined as the intersection point of $t_2$ and $t_3$.

6-2. When $P_2$ is determined, line $t_2$ that is tangent to circle $C_2$ and passes through $P_2$ is set, and $P_1$ is determined as the intersection point of $t_1$ and $t_2$.

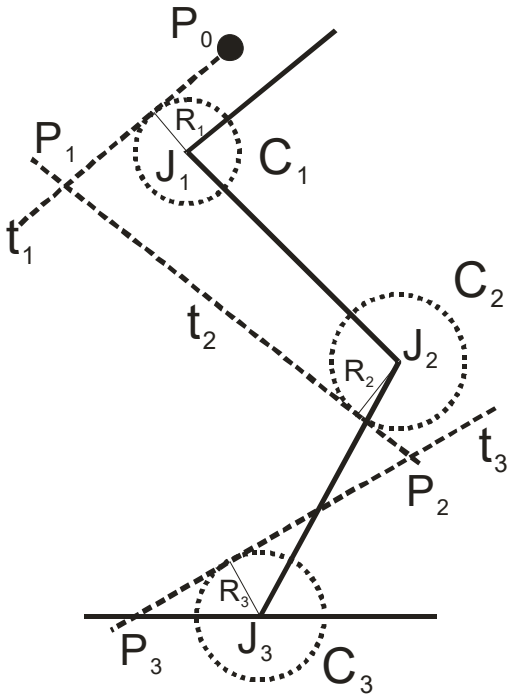


**Figure 3.** Circle $C_i$ and tangential line $t_i$.

In procedure 1, the joint angles depend on the task, such as jump and walk, that is explained in the next section. In procedures 6-1 and 6-2, the pulley position that is on line t1 or t3 can be investigated by referring to the design of the robot, such as the link size.

### *2.4. Configuration of Physical Robot*

Figure 4a shows a developed prototype of the single-legged robot for evaluating the proposed method. The links were made of light acrylonitrile butadiene styrene (ABS) and polylactide (PLA) using a 3D printer (XYZprinting Da Vinci 1.0 pro, Taiwan). The actuator was a pneumatic cylinder (SMC CDUJB6-20DM, Japan) that generated a tensional force of T = 10.0 N when the pressure of the supply air was 0.7 MPa. The lengths of the trunk, thigh, shank, and foot were 0.135, 0.11, 0.1, and 0.03 m, respectively, i.e., $l_1 = 0.135$, $l_2 = 0.11$, $l_3 = 0.1$, and $l_4 = 0.03$ m. The pulley position $P_0$ corresponding to the point generating the tensional force by the actuator and the pulley position $P_3$ corresponding to the terminal point of the wire attached on the foot were set as (-0.04, 0.275) [m] and (-0.06, 0.0) [m], respectively, when the joint angles were $\theta_1 = 0.0, \theta_2 = 0.0, \text{and } \theta_3 = \frac{\pi}{2}$ rad. Before supplying air to the actuator, three boards were attached to maintain the joint angles. These boards were separated after air was supplied; subsequently, the joints were driven. Figure 4b shows the configuration of the prototype. Note that the wire was not secured tightly for demonstration purposes. The wire and pulley were made of nylon and wood, respectively. It was assumed that no friction existed between the two.

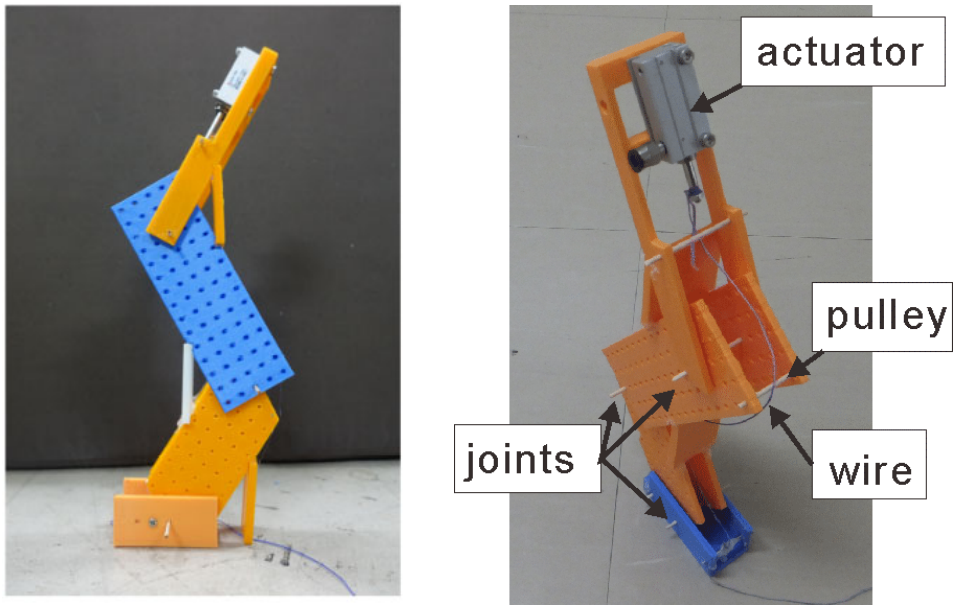


(**a**) Side view. (**b**) Configuration of prototype.

**Figure 4.** Developed three degree of freedom tendon-driven robot. (**a**) Side view; (**b**) Configuration of prototype.

The force exerted on the toe was measured using a force scale and strain gauge. Figure 5 shows the measurement setup. The horizontal force, $F_x$, was measured using the strain gauge (Nitta A201-1, Japan) attached on the toe, whereas the vertical force, $F_y$, was measured using the force scale. The maximum measurement load of the strain gauge was 4.4 N, and the nonlinear resistance to the load was measured using the 10-bit A/D converter of the microcontroller (Arduino Mega2560). Because the joint was driven and the robot moved when air was supplied to the pneumatic actuator, the robot was constrained using the gauge.

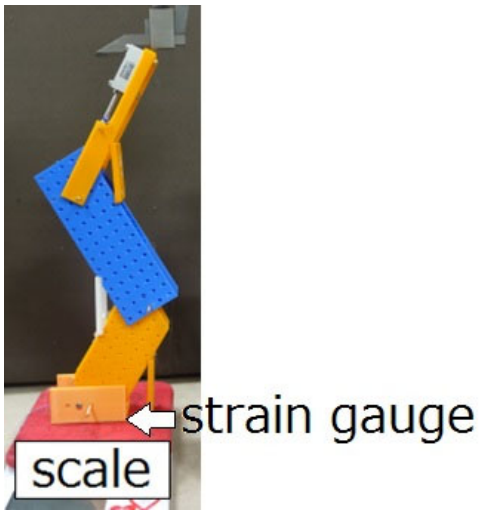


**Figure 5.** Experimental setup.

## 3. Realization of Vertical Jumping

### *3.1. Condition for Vertical Jumping*

To validate the proposed procedure that generates a force toward the desired direction, we investigated vertical jumping. The jumping motion has attracted significant attention. Some studies

have focused on insect jumping [17] and animal jumping [18]. Based on their body structures, it was discovered that the legs driven by muscles were constructed from the unique shape of the exoskeleton or bone [19,20]. This suggests that an appropriate combination of tendon-driven muscles and a flame structure provides a dexterous motion. Therefore, the structure of the robot flame is important in the tendon-driven mechanism to achieve successful motion.

To realize jumping using the proposed monopod mechanism, some assumptions were adopted: (i) The model was constrained on the sagittal plane; (ii) the interaction between the robot and ground occurred instantly, and the joint angles were not changed during the lifting off motion; (iii) and the reaction force was added at the toe. Furthermore, we assumed that the link moments were ignored. Following assumption (iii), the reaction force on the toe should be vertical, and the projection of the center of mass (CoM) on the ground should correspond to the toe; otherwise, the robot will tumble while it is in the air. To set the CoM on the ground, joint angles $\theta_1, \theta_2,$ and $\theta_3$ were determined. The joint angles were determined such that the projection of the CoM was on the toe. The angles were then set as $\theta_1 = 1.07$, $\theta_2 = -1.10$, and $\theta_3 = 2.16$ rad.

By following the procedure mentioned above, the force magnitude and direction on the toe can be designed. When the robot jumps vertically, the force should be vertical by setting the CoM over the toe, as mentioned above. In this case, the direction of the force, $\xi$, is $\frac{\pi}{2}$ rad, and Equation (4) is expressed as:

$$\begin{pmatrix} R_1 - R_2 \\ R_2 - R_3 \\ R_3 \end{pmatrix} = \mathrm{K} \begin{pmatrix} l_2 \cos(\theta_2 + \theta_3) + l_3 \cos\theta_3 + l_4 \\ l_3 \cos\theta_3 + l_4 \\ l_4 \end{pmatrix}. \quad (5)$$

By using Equation (5) and the procedure mentioned above, the pulley position can be determined.

### 3.2. Numerical Solution of Pulley Position

By setting joint angles, $\theta_1, \theta_2,$ and $\theta_3$, and pulley positions, $P_0$ and $P_3$, the geometrical conditions of $P_1$ and $P_2$ were determined by setting the vertical force, $F_y$. Figure 6 shows circle $C_i$ and tangential line $l_i$ when force $F_y$ was -7 N (Figure 6a), -4 N (Figure 6b), and -2 N (Figure 6c). T was fixed as 10 N. As shown in the figures, circle $C_i$ and tangential line $l_i$ depend on vertical force $F_y$ and tensional force T. Table 1 shows the relationship between vertical force $F_y$ and each of the radii of circles $C_1$, $C_2$, and $C_3$.

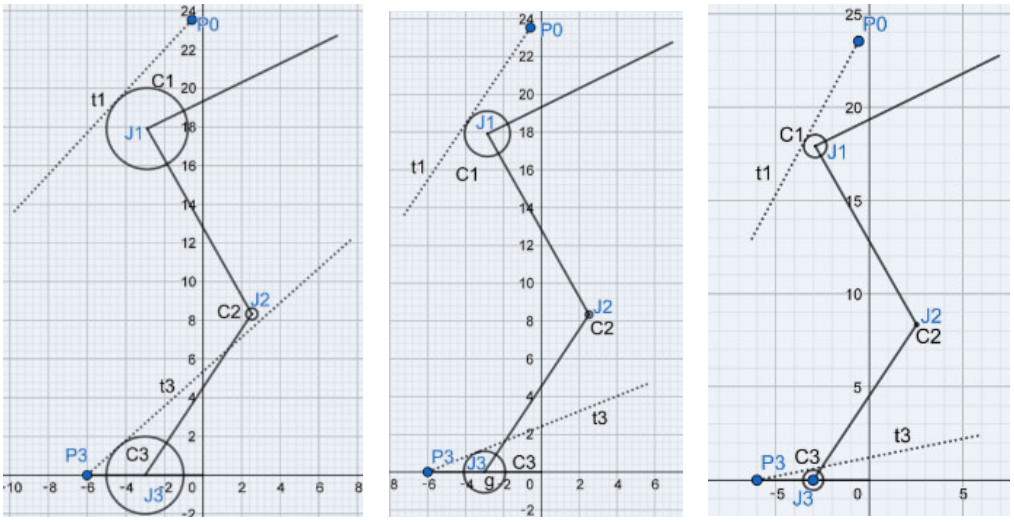


(**a**) $F_y$ = -7 N (**b**) $F_y$ = -4 N (**c**) $F_y$ = -2 N

**Figure 6.** Circle Ci and tangential line $l_i$ depending on the vertical force, $F_y$, and tensional force, T (T is fixed as 10 N). (**a**) $F_y$ = -7 N; (**b**) $F_y$ = -4 N; (**c**) $F_y$ = -2 N.

**Table 1.** Relationship between vertical force Fy and each of radii of circles $C_1$, $C_2$, and $C_3$. Tensional force T was fixed as 10 N. Units of $F_y$ and the radius are [N] and [mm], respectively.

| $F_y$ | $C_1$ | $C_2$ | $C_3$ |
|---|---|---|---|
| −9.0 | 27.6 | 3.9 | 24.6 |
| −8.0 | 24.5 | 3.5 | 21.8 |
| −7.0 | 21.4 | 3.0 | 19.1 |
| −6.0 | 18.4 | 2.6 | 16.4 |
| −5.0 | 15.3 | 2.2 | 13.6 |
| −4.0 | 12.2 | 1.7 | 10.9 |
| −3.0 | 9.2 | 1.3 | 8.2 |
| −2.0 | 6.1 | 0.9 | 5.5 |
| −1.0 | 3.1 | 0.4 | 2.7 |

### *3.3. Experiment (1): Measurement of Vertical Force*

To confirm the relevance of the pulley position that was determined based on the desired vertical force, the force was measured. The pulley position was calculated following the previous procedure using the desired force, $F_y$ ($F_y$ = -6.5, -6.8, and -8.4 N). The force was measured via the scale under the foot assuming that the force was generated on the toe. The tensional force, T, was 10 N. Table 2 shows the pulley position determined using the vertical force, and it shows the measured vertical force and the relative error between the desired and measured forces. As shown in the table, the measured vertical force almost matched the desired force. In the measurement, it was confirmed that the foot did not slide on the scale, i.e., the horizontal force, $F_x$, did not occur.

**Table 2.** Pulley position that provides desired vertical force and measured force.

| Desired $F_y$ [N] | $x_k$ [m] | $y_k$ [m] | $x_h$ [m] | $y_h$ [m] | Measured $F_y$ [N] (rel. Error [%]) |
|---|---|---|---|---|---|
| -6.5 | -0.03 | 0.09 | -0.01 | 0.24 | -6.1 (6.2) |
| -6.8 | -0.01 | 0.09 | -0.03 | 0.23 | -6.5 (4.4) |
| -8.4 | -0.03 | 0.10 | -0.04 | 0.23 | -8.4 (0.0) |

### *3.4. Experiment (2): Vertical Jumping*

By setting the pulley position, robot jumping was observed. Figure 7a shows a successful jumping when the pulley position was set following the proposed geometrical conditions: ($x_k$, $y_k$) = (-0.01, 0.09) [m], ($x_h$, $y_h$) = (-0.03, 0.23) [m], and $F_y$ = -6.8 N. For comparison, another pulley position that did not follow conditions (($x_k$, $y_k$) = (-0.01, 0.06) [m], ($x_h$, $y_h$) = (-0.03, 0.23) [m]) was tested. The jumping motion is shown in Figure 7b. As shown in Figure 7a, the knee joint lifted up to the vertical direction. This indicates that the force occurred toward the vertical direction, and then the robot jumped. Meanwhile, as shown in Figure 7b, the knee joint did not lift up toward the vertical direction, and it moved toward the horizontal direction. This indicates that the horizontal force occurred on the toe, and then the robot failed to jump. By referring to the length of the link, such as $l_3$ = 0.1 m, Figure 7a shows that the moving distance of the knee joint was approximately 33.5 mm, whereas Figure 7b shows that the moving distance of the joint was approximately 40.4 mm.

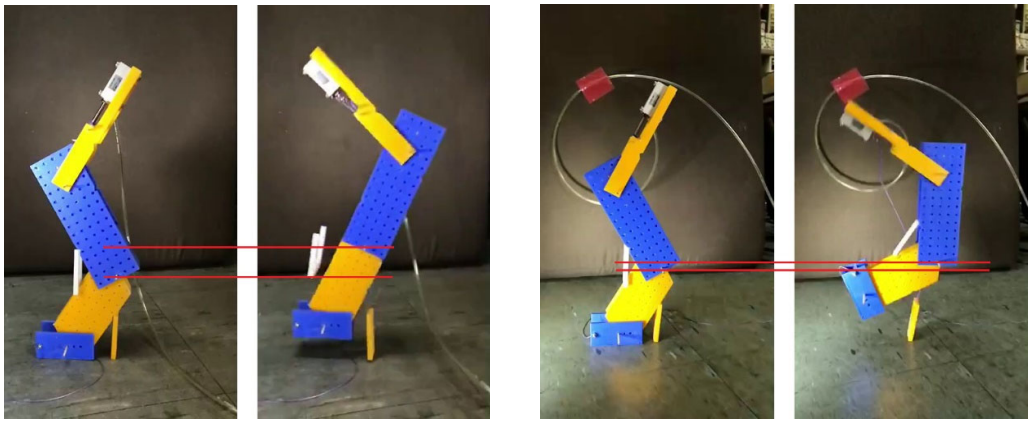

(**a**) Successful jumping. (**b**) Failed jumping.

**Figure 7.** Jumping experiment. (**a**) Successful jumping; (**b**) Failed jumping.

## 4. Generation of Force Toward Desired Direction

In the previous section, the horizontal force, $F_x$, was set to zero for the vertical jumping. In this section, we confirm that the desired force direction on endpoint $\xi$ was determined, as was $\xi = \frac{\pi}{2}$ in the previous section, by setting the appropriate pulley position. First, the direction of force $\xi$ was set; joint angles $\theta_1, \theta_2, \text{and } \theta_3$ were set; and the pulley position was calculated based on the procedure explained in Section 2. In this section, joint angles $\theta_1, \theta_2,$ and $\theta_3$ were set to the values used for the vertical jumping case because only the direction of the force on the endpoint and foot tips was discussed, and it could be generated by any posture. Figure 8 shows the trajectory of the measured horizontal force, $F_x$, when the desired forces was set to 0.25 N (Figure 8a) and 0.8 N (Figure 8b). Air was supplied into the actuator at an appropriate moment (approximately at 5 s. As shown in Figure 5, the vertical force was measured using the scale, and the horizontal force was measured using the gauge. The measurement interval was 0.1 s. As shown in the figure, the measured force converged into the desired force in each measurement. Immediately after supplying the air, the measured data did not indicate the desired value because the posture of the robot changed and a certain amount of time was required before a steady value was achieved. Because no spring–damper element existed between the foot and measurement equipment, the physical force explained in the previous section was expected to output the desired force immediately after air was supplied into the actuator.

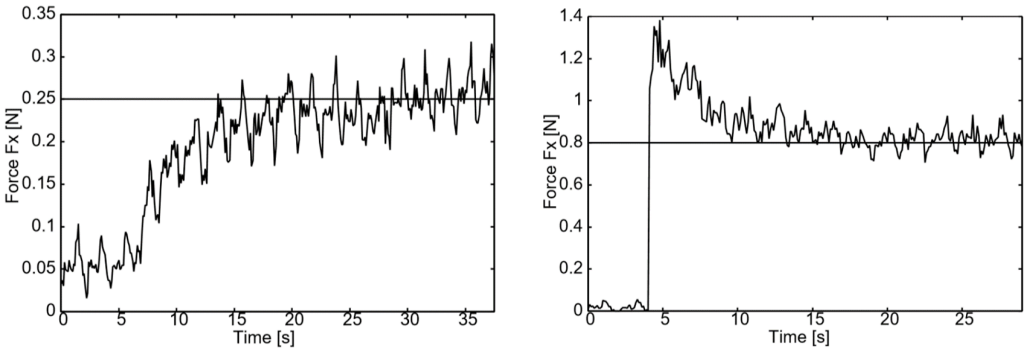


(**a**) Fx = 0.25 N. (**b**) Fx = 0.8 N.

**Figure 8.** Measured and desired force Fx (0.25 and 0.8 N, respectively). (**a**) Fx = 0.25 N; (**b**) Fx = 0.8 N.

Additional experiments were conducted when the desired forces, $F_x$, were set 0.3, 0.4, and 0.5 N, as well as 0.25 and 0.8 N. First, the set of diagonal forces, $F_x$ and $F_y$, or that of the force magnitude, F, and the tangential angle of the force, $\xi$, were determined. In this experiment, $F_x$ and $F_y$ were

determined. Subsequently, the pulley position was based on the procedure explained in Section 2.3. Table 3 shows the desired forces, $F_x$ and $F_y$, and the tangential angle $\xi$ obtained by calculating $\xi = \tan^{-1}(\frac{F_x}{F_y})$, corresponding position of pulleys, measured forces, and relative error between the desired and measured forces. The measured forces were obtained by recording and averaging 20 measurement values (2 s) before the measurement was halted. As shown in the table, the measured $F_x$ and $F_y$ matched the desired forces.

**Table 3.** Pulley position that provides desired forces and measured force.

| Number | Desired $F_x$ [N] / $F_y$ [N] | $\xi$ [rad] | $x_k$ [m] / $y_k$ [m] | $x_h$ [m] / $y_h$ [m] | Measured $F_x$ [N] (rel. Error [%]) / $F_y$ [N] (rel. Error [%]) |
|---|---|---|---|---|---|
| 1 | 0.25 | 1.53 | −0.02 | −0.04 | 0.26 (4.0) |
| | −5.8 | | 0.09 | 0.23 | −5.9 (1.7) |
| 2 | 0.3 | 1.52 | −0.01 | −0.01 | 0.31 (3.3) |
| | −5.5 | | 0.08 | 0.24 | −5.7 (3.6) |
| 3 | 0.4 | 1.51 | −0.02 | −0.05 | 0.44 (10.0) |
| | −7.1 | | 0.09 | 0.24 | −7.1 (0.0) |
| 4 | 0.5 | 1.50 | −0.01 | −0.05 | 0.51 (2.0) |
| | −7.0 | | 0.08 | 0.24 | −5.9 (15.7) |
| 5 | 0.8 | 1.39 | −0.01 | −0.04 | 0.83 (3.8) |
| | −4.4 | | 0.08 | 0.24 | −4.3 (2.3) |

## 5. Conclusions

Herein, the geometrical condition of a tendon-driven mechanism was derived. Based on specified conditions, the procedure to determine the pulley position for generating the desired angle and magnitude of reaction force on the toe was proposed. To achieve the desired angle and force magnitude, Higashimori's equation of the wire-driven mechanism by a single actuator was adopted and revised. The equations to generate the desired horizontal and vertical forces were derived. To evaluate the proposed method, we analyzed vertical jumping. The conditions of vertical jumping were as follows: The projection of the CoM before jumping was set on the toe, and a horizontal force should not be generated. For the first condition, the posture of the robot was determined. For the second condition, the proposed approach was applied by setting a vertical force angle, i.e., the horizontal force was set to zero, and the pulley position was determined by setting the magnitude of the desired vertical force. In the experiment, a single-legged robot driven by the single pneumatic actuator and wire was developed. The pulley was set based on the proposed approach, and it was confirmed that the measured and designed vertical forces matched. The robot achieved vertical jumping. To evaluate a general situation, the proposed approach was applied to realize the desired direction and magnitude of the force. In the physical experiment, it was confirmed that a force occurred toward the desired direction and magnitude of the force by setting the appropriate pulley position. By using this method, a robot driven by a single actuator and wire is expected to accomplish many tasks, enabled by the appropriate pulley position based on the task.

However, the proposed method has some limitations. We assumed that the radius of the pulley was negligible for simplifying Higashimori's model. Therefore, a force error can occur when the radius of the pulley cannot be ignored. This does not guarantee that all derived positions are within the area of the link, i.e., a certain pulley is far from the joint. The arrangement of the pulley in which the tendon is in contact with the link should be avoided. This paper did not discuss the friction between the pulley and tendon, i.e., the materials used for the tendon and pulley were not mentioned. Based on a study by Lai et al. [21], it is known the friction between the pulley and tendon is crucial for tension transmission. They will be discussed as an extension of the proposed method in the future.

**Acknowledgments:** This study was supported in part by JSPS KAKENHI Grant Number 19H04193. The author would like to thank Y. Sekine, F. Kitaura, and K. Takai for their technical assistance with the experiments and analysis.

**Conflicts of Interest:** The authors declare no conflict of interest.

## References

1. Xu, Z.; Kumar, V.; Todorov, E. A low-cost and modular, 20-DOF anthropomorphic robotic hand: Design, actuation and modeling. In Proceedings of the 2013 13th IEEE-RAS International Conference on Humanoid Robots (Humanoids), Atlanta, GA, USA, 15–17 October 2013; pp. 368–375.
2. Higashimori, M.; Kaneko, M.; Namiki, A.; Ishikawa, M. Design of the 100G capturing robot based on dynamic preshaping. *Int. J. Robot. Res.* **2005**, *24*, 743–753.
3. Songac, S.; Lib, Z.; Yua, H.; Ren, H. Shape reconstruction for wire-driven flexible robots based on Bézier curve and electromagnetic positioning. *Mechatronics* **2015**, *29*, 28–35.
4. Iii, R.J.W.; Jones, B.A. Design and Kinematic Modeling of Constant Curvature Continuum Robots: A Review. *Int. J. Robot. Res.* **2010**, *29*, 1661–1683.
5. Liu, T.; Mu, Z.; Xu, W.; Yang, T.; You, K.; Fu, H.; Li, Y. Improved Mechanical Design and Simplified Motion Planning of Hybrid Active and Passive Cable-Driven Segmented Manipulator with Coupled Motion. In Proceedings of the 2019 IEEE/RSJ International Conference on Intelligent Robots and Systems (IROS), Macau, China, 4–8 November 2019; pp. 5978–5983.
6. Wei, Z.; Song, G.; Zhang, Y.; Sun, H.; Qiao, G. Transleg: A wire-driven leg-wheel robot with a compliant spine. In Proceedings of the 2016 IEEE International Conference on Information and Automation (ICIA), Ningbo, China, 1–3 August 2016; pp. 7–12.
7. Kitano, S.; Hirose, S.; Horigome, A.; Endo, G. TITAN-XIII: Sprawling-type quadruped robot with ability of fast and energy-efficient walking. *Robomech J.* **2016**, *3*, 1–16.
8. Spröwitz, A.; Ajallooeian, M.; Tuleu, A.; Ijspeert, A. Kinematic primitives for walking and trotting gaits of a quadruped robot with compliant legs. *Front. Comput. Neurosci.* **2014**, *8*, 1–13.
9. Seok, S.; Wang, A.; Chuah, M.Y.; Otten, D.; Lang, J.; Kim, S. Design Principles for Highly Efficient Quadrupeds and Implementation on the MIT Cheetah Robot. In Proceedings of the 2013 IEEE International Conference on Robotics and Automation, Karlsruhe, Germany, 6–10 May 2013; pp. 3307–3312.
10. Yamaguchi, T.; Ambe, Y.; Ando, H.; Konyo, M.; Tadakuma, K.; Maruyama, S.; Tadokoro, S. A Mechanical Approach to Suppress the Oscillation of a Long Continuum Robot Flying with Water Jets. In Proceedings of the 2019 IEEE/RSJ International Conference on Intelligent Robots and Systems (IROS), Macau, China, 4–8 November 2019.
11. Li, Z.; Wu, L.; Ren, H.; Yu, H. Kinematic comparison of surgical tendon-driven manipulators and concentric tube manipulators. *Mech. Mach. Theory* **2017**, *107*, 148–165.
12. Viau, J.; Chouinard, P.; Bigue, J.-P.L.; Julio, G.; Michaud, F.; Shimoda, S.; Plante, J.-S. Projected PID Controller for Tendon-Driven Manipulators Actuated by Magneto-Rheological Clutches. In Proceedings of the IEEE/RSJ International Conference on Intelligent Robots and Systems, Hamburg, Germany, 28 September–2 October 2015; pp. 5954–5959.
13. Chen, T.; Haas-Heger, M.; Ciocarlie, M.T. Underactuated Hand Design Using Mechanically Realizable Manifolds. In Proceedings of the 2018 IEEE International Conference on Robotics and Automation (ICRA), Brisbane, Australia, 21–25 May 2018; pp. 7392–7398.
14. Takuma, T.; Takai, K.; Iwakiri, Y.; Kase, W. Body design of tendon-driven jumping robot using single actuator and wire set. In Proceedings of the 21st International Conference on Climbing and Walking Robots and Support Technologies for Mobile Machines (CLAWAR 2018), Panama City, Panama, 9–12 September 2018; pp. 93–100.
15. Rombokas, E.; Theodorou, E.; Malhotra, M.; Todorov, E.; Matsuoka, Y. Tendon-Driven Control of Biomechanical and Robotic Systems: A Path Integral Reinforcement Learning Approach. In Proceedings of the 2012 IEEE International Conference on Robotics and Automation, Saint Paul, MN, USA, 14–18 May 2012; pp. 208–214.
16. Inouye, J.M.; Valero-Cuevas, F.J. Anthropomorphic tendon-driven robotic hands can exceed human grasping capabilities following optimization. *Int. J. Robot. Res.* **2014**, *33*, 694–705.
17. Nabawy, M.R.A.; Sivalingam, G.; Garwood, R.J.; Crowther, W.J.; Sellers, W.I. Energy and time optimal trajectories in exploratory jumps of the spider *Phidippus regius*. *Sci. Rep.* **2018**, *8*, 1–15.

18. McGowan, C.P.; Baudinette, R.V.; Usherwood, J.R.; Biewene, A.A. The mechanics of jumping versus steady hopping in yellow-footed rock wallabies. *J. Exp. Biol.* **2005**, *208*, 2741–2751.
19. Burrows, M. Anatomy of the hind legs and actions of their muscles during jumping in leafhopper insects. *J. Exp. Biol.* **2007**, *210*, 3590–3600.
20. Hildebrand, M. The Mechanics of Horse Legs. *Am. Sci.* **1987**, *75*, 594–601.
21. Lai, W.; Cao, L.; Tan, R.X.; Tan, Y.C.; Li, X.; Phan, P.T.; Tiong, A.M.H.; Tjin, S.C.; Phee, S.J. An Integrated Sensor-Model Approach for Haptic Feedback of Flexible Endoscopic Robots. *Ann. Biomed. Eng.* **2020**, *48*, 342–356.